ME301 project 2025 GROUP 36

✉ **Email addresses:**
[1]cesar.villa@epfl.ch
[2]guillaume.masclet@epfl.ch
[3]maxence.latrouite@epfl.ch
[4]romain.heinzer@epfl.ch

Villa, César[1]
Masclet, Guillaume[2]
Latrouite, Maxence[3]
Heinzer, Romain[4]

Sciper numbers:
[1]334551
[2]346163
[3]346782
[4]331655

Abstract

This experiment is inspired by our shared interest in sailing and desire to study the physics of a sailboat.

Our motivation stems from our wish to understand the dynamics of active ballast transfer, an emerging anti-roll technology adapted for small boats. To understand the dynamics involved in a sudden wind lull and in steady flow conditions, we propose a simplified model.
This reduced scale experimental setup uses an aquarium. At one end is a fan generating constant airflow. On the sides are supports for a rotating model boat made of a hull, keel and mast with sails.
This allows us to record the deflection of the mast with a camera, the rolling motion with an accelerometer, and the force applied by the wind with a load cell.
The most prominent challenge is avoiding an overdamped system and maintaining visible oscillation while minimizing signal noise, working in a wet environment. This experiment proves that oscillatory behavior is an important component of sailboat dynamics and that deflection is a phenomenon that should be taken into consideration.

Overall, the setup effectively simulates the behavior of a real sailboat on a smaller scale, and allows the study of steady state and oscillatory behavior.

1 Motivation

Due to forces applied on the sails by wind flows, all sailboats are prone to mast deflection, inclination, and oscillatory behavior. This represents a major design consideration, and an important factor in the wear and tear of equipment and the safety of users. It is also an important consideration in the design of new technologies such as active ballast transfer. This technology seeks to counteract roll by shifting water between tanks on small boats. Understanding roll is essential to effectively design technological advancements.
The impact of environmental conditions on the mechanics and dynamics of sailboats is an extremely wide subject, which is why we decided to focus on a few commonly observed phenomena.

Oscillatory behavior can be observed in many ways on a sailboat. To narrow down our area of research, we focus on the rolling motion often observed as a consequence of a sudden wind lull or when passing through a wind shadow. The end goal being to study both its oscillatory behavior and the nature of forces induced at the base of the mast. Understanding oscillatory behavior is a critical step in designing active ballast transfer systems.
Another important design consideration resides in the behavior of the mast when a constant wind force is applied, i.e. while sailing in regular wind conditions. A mast's long, narrow shape inevitably causes deflection not dissimilar to that of a beam. This idea is reinforced when considering that sails are usually attached to a few select points along the mast. A steady wind applied on a mast and sails can then be studied as a classic structural mechanics problem with a clamped beam subject to point forces, which raised our interest. We also decided to take into account the steady force applied at the bottom of the mast by a steady wind flow.

2 Experimental set-up

2.1 Experimental system description

Our system consists of a rectangular aquarium acting as a tank. Two rigid mounts are fixed to the opposite long edges; each mount can operate either in free mode via a shaft mounted on ball bearings, providing almost friction-free roll, or in locked mode thanks to a screw that prevents the shaft from rotating. The two shafts are rigidly connected to a model hull positioned at the center of the tank. The hull is equipped with:

- a mast carrying a sail;
- a ballast keel.

On one short wall of the aquarium, a 24 V axial fan is installed so as to generate an airflow perpendicular to the sail. The aerodynamic moment produced rolls the hull about the shafts.

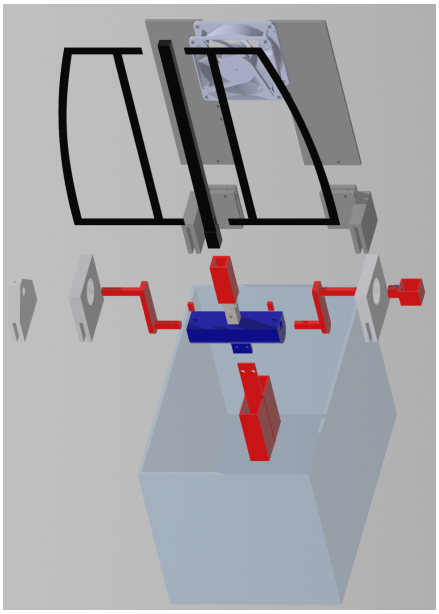

Figure 1: Exploded view of the set-up.

Instrumentation:

- **MMA 8451 accelerometer** mounted on one of the shafts → real-time measurement of the inclination angle.
- **5 kg load cell** clamped at the foot of the mast → measurement of the thrust exerted by the wind on the sail.
- **GoPro 11 Mini camera** placed at the side of the tank → tracking of black points to determine the lateral deflection of the mast.

This configuration allows repeatable acquisition of roll angle, aerodynamic force and mast bending under a controlled wind, ensuring the repeatability of the tests.

2.2 Operating protocol

1. **Filling the aquarium**
   - Add water until the hull is exactly level with the surface.
2. **Installation of the model boat**
   - Fix the free boat mounts to the long edges of the aquarium, 9 cm away from the edge opposed to the fan mounts. Attach the model hull and keel to the supports.
   - Rigid mast: install the PETG printed mast to the hull for rigidity tests.
3. **Switching on the fan**
   - Before switching the fan on, perform a zero-offset calibration on sensors.
   - Connect the 24 V DC fan to the bench power supply.
   - Set the supply to 24 V (current limit 1.5 A) and switch on.
   - Wait ~5 s for the airflow to stabilise.
4. **First data acquisition**
   - Start the Arduino data-collection program.
   - Shut off the wind:
     - **Accelerometer:** measures the oscillation of the inclination angle (°) after the shut off.
     - **Load cell:** measures the oscillatory forces at the bottom of the mast caused by the oscillation of the hull after the shut off.
   - Record data for ~10 s at steady state, then stop acquisition and save the files.
   - Switch the fan back on and repeat the procedure ten times.
5. **Change of setup**
   - Change the free supports for the fixed ones.
   - Change the rigid PETG mast for the flexible TPU.
6. **Second data acquisition**
   - Place the camera on its support at its calibrated distance to ensure repeatability.
   - Turn on the camera and calibrate it using a grid square pattern to account for lens distortion.
   - Turn the fan back on.
   - Start recording: the camera measures the steady state deflection of the mast.
   - Record data for ~10 s at steady state, then stop acquisition and save the files.
   - Switch off the fan and disassemble the setup
   - Upload the video to matlab for post-treatment of deflection values.

This protocol ensures that every test is carried out under identical geometric and aerodynamic conditions, guaranteeing comparability and reproducibility of the measurements.

3 Camera setup : Deflection of the mast

3.1 Description

The first measurement setup uses a GoPro Hero11 Mini as an optical sensor to record the deflection of the mast. The camera is mounted on a rigid tripod at a fixed height and precisely positioned on a marked wooden board, ensuring a constant stand-off distance and orientation across all tests.

The mast is equipped with 15 evenly spaced black markers, and the deflection is filmed in 2.7K at 240 fps, offering both high spatial resolution (enabling subpixel precision) and high temporal sampling.

After recording, a calibration step is performed using a reference grid placed at the mast position. The calibration procedure in MATLAB computes the camera matrix and distortion coefficients, which are then used to rectify each frame and transform pixel coordinates into real-world metric positions. After processing, the rectified marker trajectories are exported as `.csv` files and plotted in Matlab, where the mean deflection profile with its point-wise standard deviation is displayed. The analysis proceeds as follows:

1. **Manual selection** of the 15 markers on the initial frame;
2. **Automatic tracking** of these points across frames using a custom MATLAB script;
3. **Geometric rectification** of all tracked positions using the calibration matrix;
4. **Extraction of the steady-state regime** by selecting a set of ∼50 frames during which the motion stabilizes (minimal point displacement);
5. **Polynomial fitting** of the mean deflected shape using a third-order polynomial (`polyfit`) to estimate the curvature profile of the mast.

3.2 Results

The mast deflection was recorded in 2.7 K mode (2704×1520 px) at 240 fps. The camera was positioned at a stand-off distance of $d = 0.25\,\mathrm{m}$ and tilted by $\alpha = 30°$ with respect to the mast´s axis. A full pinhole calibration (camera matrix K and distortion coefficients) corrects the perspective projection; after rectification the scale factor at the mast plane is $s = K^{-1} \approx 0.36\,\mathrm{mm\,px^{-1}}$. Combined with a sub-pixel centroid algorithm (1/8 px), the resulting position resolution is $\sigma_x = s/8 \simeq 0.045\,\mathrm{mm}$.

Ten full experiments were conducted under identical conditions. The resulting deflection profiles Δx [cm] are presented in Figure 2 as a function of the distance to the base of the mast z [cm], along with the pointwise standard deviation.

The left panel shows the close alignment of all ten profiles, which follow a highly consistent trajectory. The right panel provides a close-up at the mast tip, where the spread is most pronounced. The grey shaded area represents the standard deviation between trials. Despite the independent repetitions, the spread remains under 2 mm in the worst case. The black curve corresponds to the mean deflection profile across all trials.

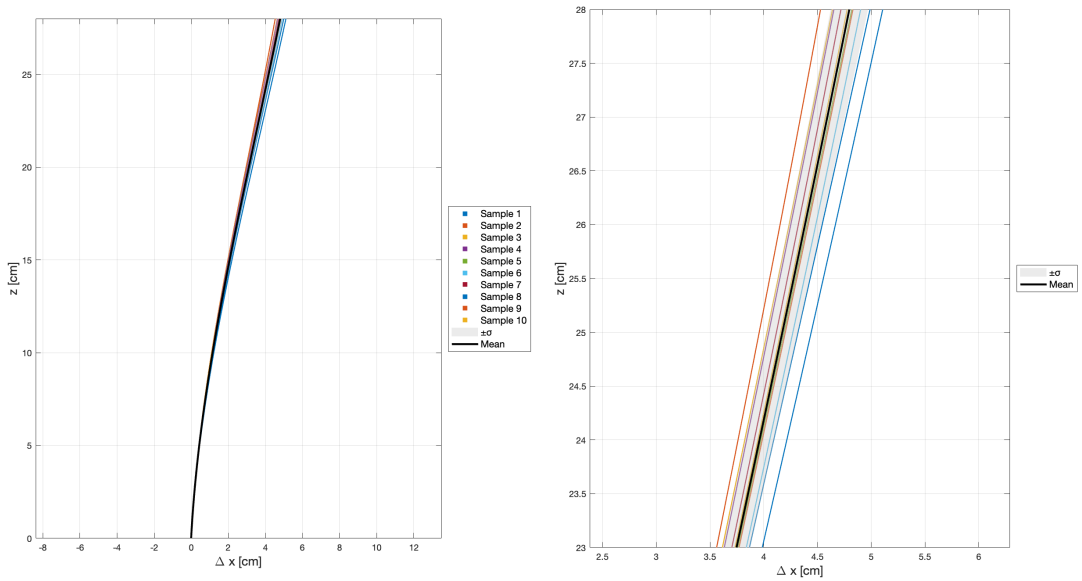

(a) Full-Length Shape Comparison Across Trials **(b)** Tip Region Analysis

Figure 2. Analysis of Mast Deflection Profiles Using Polynomial Fitting

The standard deviation between the ten trials reaches a maximum of

$$\sigma_{\text{inter}}^{\max} = 0.1730 \text{ cm},$$

i.e. 1.73 mm at the tip of the mast, which corresponds to 3.46% of the maximum deflection amplitude (about 5 cm).

Sample	Fitting equation	RMSE [cm]
1	$x = -0.000119\,y^3 + 0.00785\,y^2 + 0.056\,y - 0.00828$	0.0215
2	$x = -0.00013\,y^3 + 0.00741\,y^2 + 0.0456\,y + 0.00913$	0.0299
3	$x = -0.000125\,y^3 + 0.00743\,y^2 + 0.0485\,y + 0.0151$	0.0221
4	$x = -0.000103\,y^3 + 0.00742\,y^2 + 0.0555\,y + 0.0663$	0.024
5	$x = -0.00013\,y^3 + 0.00746\,y^2 + 0.0574\,y + 0.0705$	0.0225
6	$x = -0.000113\,y^3 + 0.00738\,y^2 + 0.0599\,y + 0.0185$	0.0252
7	$x = -0.000107\,y^3 + 0.00745\,y^2 + 0.0535\,y - 0.00165$	0.0247
8	$x = -0.000113\,y^3 + 0.00743\,y^2 + 0.0524\,y - 0.0106$	0.03
9	$x = -0.000113\,y^3 + 0.00738\,y^2 + 0.0521\,y - 0.0202$	0.0272
10	$x = -0.000111\,y^3 + 0.00732\,y^2 + 0.0535\,y - 0.00726$	0.022
Mean	$x = -0.000111\,y^3 + 0.00732\,y^2 + 0.0535\,y - 0.00726$	–

Table 1. Polynomial fitting equations and RMSE for each mast deflection sample

The table above shows the fitted polynomial equations for each of the ten mast deflection measurements, as well as the corresponding RMSE values. We observe that the equations are very similar from one run to another, which confirms that the experimental

setup produced highly consistent results. The RMSE values are all low—mostly between 0.02 and 0.03cm—indicating that the cubic polynomial model captures the shape of the mast very accurately. The mean fit, computed from the average of all profiles, aligns closely with the individual fits and provides a reliable representation of the mast's typical deflection under loading.

To assess the reliability of the mast deflection measurements, we identified and quantified the main sources of uncertainty. First, we tested the variability induced by manual tracking by repeating the point selection several times on the same trial, deliberately clicking on extreme pixel positions for each marker. Despite this, the resulting differences led to a maximum deviation of 0.79 mm at the mast tip and an average of 0.74 mm across the height, corresponding to only 1.6% of the total deflection.

Additional sources of uncertainty were also considered. The sensor resolution, at a scale of 0.36 mm/px and with subpixel centroiding (1/8 pixel), limits positional accuracy to approximately ± 0.045 mm, i.e., less than 0.1% of the 50 mm deflection. A potential out-of-plane perspective error, due to imperfect alignment of the calibration grid with the mast's deflection plane, was estimated by assuming a tilt of 2°, resulting in a lateral geometric bias of about 0.17 mm (0.3%). Lastly, residual distortion in the calibration process—as seen in the reprojection error—was conservatively estimated to contribute up to 1%.

Overall, when combining these factors, the total uncertainty affecting the measured mast deflection remains under approximately 2%, confirming the robustness of the measurement method and the reliability of the extracted profiles.

4 Load Cell: steady-state and oscillating values

4.1 Description

For the purpose of measuring the steady state force applied on the sails as well as the oscillating force when the wind stops, a 5 kg loadcell and an amplifier are used. The weights of the mast, the sails and the wind can create a combined force superior to 1 kg, which is why we discarded the 1 kg loadcell. A 5 kg loadcell is sufficient in our case.
It is clamped to the hull at one end, and holds the mast at the other through a connector. This design ensures that the mast stays rigidly clamped to the hull while at the same time transmitting the entirety of the force through the load cell.
The load cell is made of a metal body, strain gauges, and an electrical circuit. The deformation of the body and the strain gauges create a voltage output proportional to the applied force using the electrical circuit. The output signal is of the order of a few millivolts and requires amplification through a signal conditioner.
The load cell's input range spans from 100 g to 5200 g, with a total span of 5100 g. The output range varies from 0.6 mVN ± 0.15 to 1.0 mV/V ± 0.15. For the maximum measured value of 5200 g, the resolution of the load cell is 91 μg , with a dynamic range of $16.8{\times}10^6$.

Given that the system exhibits rapid oscillations over an average duration of 8 seconds, it was essential to capture high-resolution temporal data. To achieve this, we employed an amplifier capable of increasing the data acquisition rate from the default 10 Hz to 80 Hz, allowing more detailed tracking of the system's dynamic behavior during the measure-

ment window. This adjustment increases the input noise from 50 to 90 nV(rms). With our 24-bit signed ADC, an input noise of 90 nV (rms) corresponds to approximately 302 digital counts (rms), which is consistent with the observed signal fluctuations in the raw data. Given the full-scale range of 5 mV, the resolution of the 24-bit signed ADC is approximately 0.298 nV per digital step.

4.2 Results

We repeat the experiment ten times to obtain comparable data samples. As the experiment is repeated in the same conditions, we can expect similar load curves. We choose to plot the data with normalized, non-dimensional values $\frac{P}{P_\infty}$ across time t [s]. P is the load generated by oscillation and P_∞ is the steady state applied load. We are interested in the oscillatory behavior, while the specific load values are features of the setup and present little interest to our study.
To assess the quality of our experimental protocol, we compute three key parameters: the global mean μ_{global}, the global standard deviation σ_{global}, and the coefficient of variation (CV). Both μ_{global} and σ_{global} are calculated from the raw load-cell data, prior to rescaling the signal to a percentage of the preload and re-centering it so that the steady-state level is set to 0 %.

$$\text{CV} = \frac{\sigma_{\text{global}}}{\mu_{\text{global}}}$$

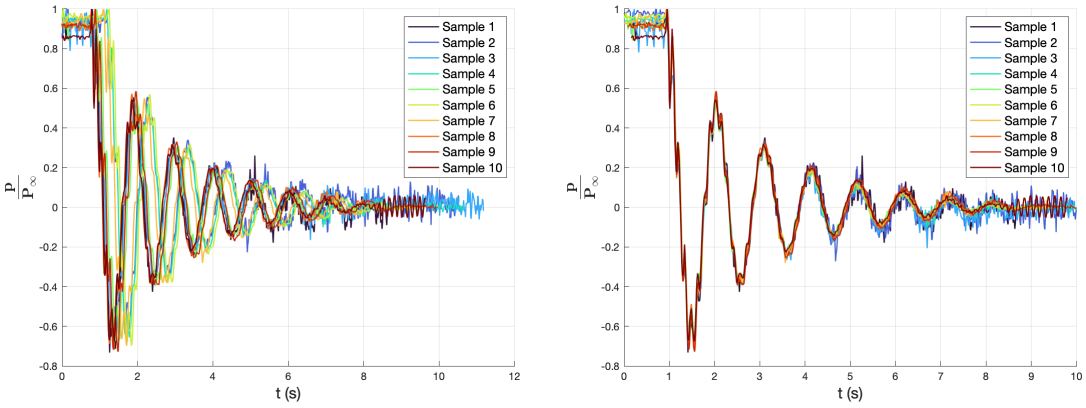

(a) Before synchronizing sets

(b) After synchronizing sets

Figure 3. Unsynchronized and synchronized measures from the loadcell

Sample values are not initially aligned with reference to time. To superimpose them, we detect the principal peak in every curve and shift the corresponding time axis so that all peaks coincide before further analysis.

To better understand the significance of our samples, they are averaged in the curve μ. The standard deviation σ is plotted alongside μ with $\mu + \sigma$ and $\mu - \sigma$. We also plot the smoothed values with the average $\mu_{smoothed}$, $(\mu + \sigma)_{smoothed}$ and $(\mu - \sigma)_{smoothed}$ in this configuration.

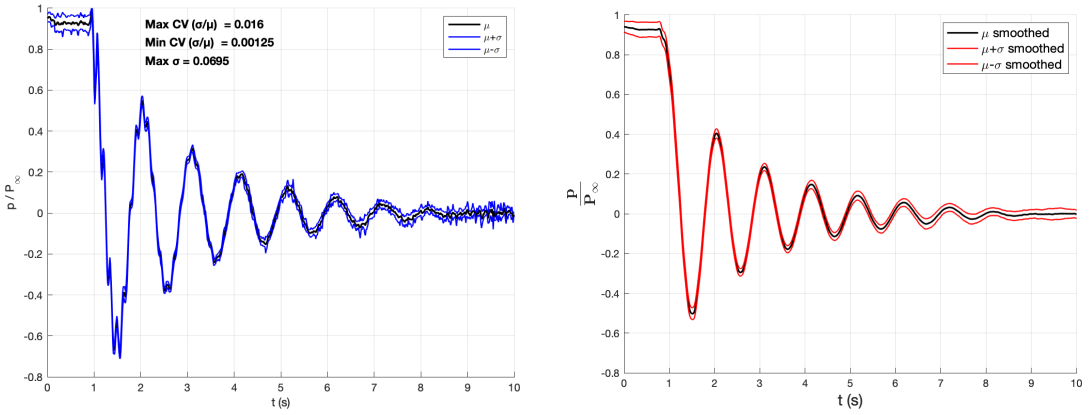

(a) Mean and standard deviation with noise

(b) Smoothed mean and standard deviation

Figure 4. Mean and standard deviation of the loadcell sets

The ten times repeated load-cell acquisitions exhibit the repeatability of the experiment, with the coefficient of variation never exceeding 1.6 %. Such a low CV indicates that the standard deviation of each series represents only a very small fraction of its mean value, confirming that random noise and experimental scatter are practically negligible. In practical terms, the load-cell output is stable to within ±1.4 % of the nominal signal across all trials, well inside the ±5 % threshold commonly adopted as a benchmark for high-precision force measurements.

We observe the convergence of sample values to 0 as the boat settles back to equilibrium, with the mast in a vertical position. The mast's self weight is perpendicular to the horizontal axis of measurement of the load cell, which is why the load value converges to zero.

Potential Sources of Error in Load Cell Measurements

Load cells are typically calibrated for force along a specific axis. Twisting forces from uneven wind flows or imperfections in the symmetry of the sails can introduce measurement errors. This may reduce the accuracy of the measurement. Our system is mostly safe from this, as we designed symmetrical sails and the fan provides a constant wind flow at 24V. This could however be the cause of part of the noise.

The mast's natural vibration may provide false peaks to the data, or create destructive interference with the boat's oscillation. The use of a rigid mast for the measurement prevents the mast's from overtaking the boat's by limiting the potential amplitude of said vibrations. This prevents this issue from impacting the samples beyond signal noise that is filtered out when processing the data.

5 Accelerometer: Oscillating values

5.1 Description

The MMA8451 accelerometer is a 3-axis digital accelerometer based on capacitive transduction, where a suspended internal mass shifts under acceleration, changing the distance between capacitor plates. This variation in capacitance alters an electrical signal,

which is then filtered and digitized within the sensor. The output is a stable digital signal providing acceleration data in m/s^2 along the x, y, and z axes.

In our experiment, the accelerometer is positioned at the center of rotation of the boat's hull, with the z-axis oriented vertically along the mast and the y-axis aligned with the mast's bending direction. This setup was chosen to ensure that the sensor would only measure static acceleration due to gravity, avoiding interference from dynamic effects. This allows us to compute the mast's inclination angle directly using the arc tangent of the ratio between y and z axis accelerations, a_y and a_z. The angle ϕ can be calculated using the following expression:

$$\phi = \arctan(\frac{a_y}{a_z}) \times \frac{180}{\pi} \tag{1}$$

The accelerometer is connected to an Arduino Uno using the I2C protocol. The Arduino handled signal acquisition and basic conditioning, transmitting the data to MATLAB via a serial interface in a custom format. To maintain temporal alignment with the load cell measurements, the system operates at a sampling rate of 80 Hz, sufficient for tracking slow oscillations of the mast while ensuring synchronized data across sensors.

5.2 Results

The MMA8451 is configured with an input range of ±2 g, giving a total input span of 4 g. The sensor has a 12-bit resolution, corresponding to 4096 discrete levels. This results in a resolution of 0.0078125 g per bit. Given the small and slow oscillations of the mast, this resolution is well suited to our application.

The output data is transmitted digitally in acceleration units (m/s^2) and processed in MATLAB to compute the inclination angle. The output span remains within ±2 g, and no saturation or clipping occurred during the measurement sessions.

The dynamic range of the sensor is approximately 60.2 dB, enabling reliable detection of subtle angular variations. The sensor shows good sensitivity and stability throughout the experiment. Minor variations in the signal at rest are observed and can be attributed to electrical noise or quantization effects from the ADC. However, these errors remain negligible and do not impact the accuracy of the angle calculation. Overall, the characteristics of the accelerometer are well suited to the needs of the measurement task.

Sample values are not initially aligned with reference to time. To superimpose them, we detect the principal peak in every curve and shift the corresponding time axis so that all peaks coincide before further analysis (Fig. 5a).

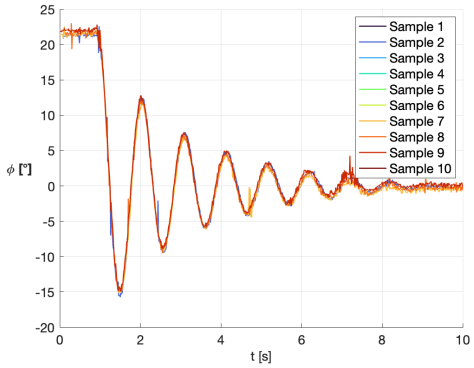

(a) Synchronized sets

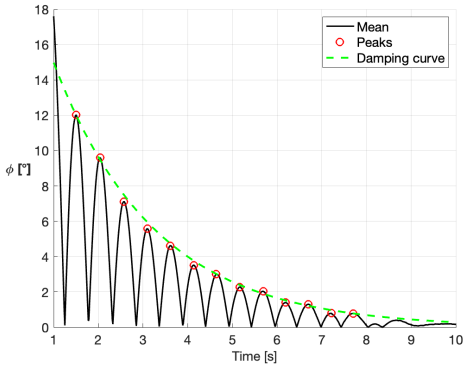

(b) Mean of signals in absolute value and damping

Figure 5. Synchronized sets and damping curve

To better understand the significance of our samples, they are averaged in the curve μ. The absolute value of μ is taken and plotted alongside the damping curve (Fig. 5b).

The damping ratio ζ of the system is computed using MATLAB based on the decay of successive oscillation peaks in the measured response, illustrated in Figure 5b, the logarithmic decrement method is applied. This yields a damping ratio of 8.95 %, indicating a lightly damped second-order system. This value of damping implies that oscillations decay gradually without excessive overshoot or instability.

The standard deviation σ is plotted alongside μ with $\mu+\sigma$ and $\mu-\sigma$ (Fig. 6a). We also plot the smoothed values with the average $\mu_{smoothed}$, $(\mu+\sigma)_{smoothed}$ and $(\mu-\sigma)_{smoothed}$ (Fig. 6b).

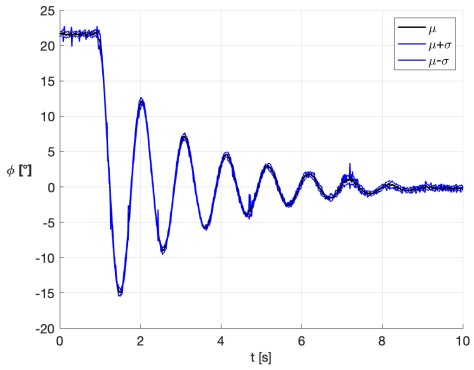

(a) Mean and standard deviation with noise

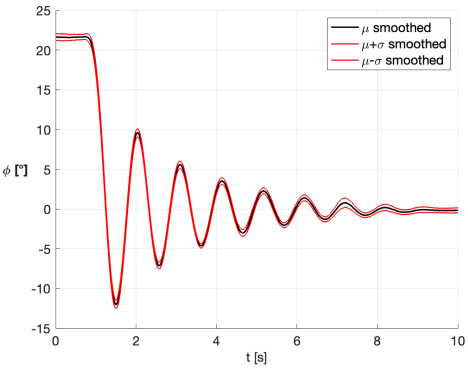

(b) Smoothed mean and standard deviation

Figure 6. Mean and standard deviation of the accelerometer

The accelerometer provides ostensibly comparable, yet smoother curves than the load cell.

It is important to note that the accelerometer is precise enough that we can consider its values as the real oscillation. Comparatively, the load cell is suitable to observe the oscillatory nature of the setup, although at a lesser degree of precision, but only the accelerometer can be used for a precise study of amplitudes.

6 Digital signal processing

To analyze the angular response of our system sampled at 80 Hz, we first interpolate and center the raw signal, then apply zero-phase Butterworth filters (low-pass followed by high-pass). In the time domain (Fig. 7c), the gray trace shows the centered raw data, while the blue trace displays the filtered result: slow drifts and high-frequency noise are effectively removed, revealing a clean, damped oscillation. The amplitude of the filtered signal is denoted by K. The initial segment of the filtered signal is not flat due to the high-pass filter, which removes low-frequency and constant components, including the initial steady-state level.

We next compute the Fast Fourier Transform (FFT) of both signals and plot their amplitudes on a linear scale (Fig. 7b). The light-blue curve corresponds to the FFT of the centered raw signal, and the red curve to the FFT of the filtered signal. Here, the amplitude values are expressed in terms of the unit of the load cell. It is clear that almost all spectral energy above the automatically determined cutoff (1.1 Hz) has been effectively suppressed.

Finally, we apply a Hann window to the centered signal and plot its single-sided spectrum in decibels (Fig. 7a). The narrow peak near 1 dB identifies the dominant frequency—measured at 0.97 Hz—while the noise floor around –40 to –60 dB confirms that unwanted components have been relegated well below the main response.

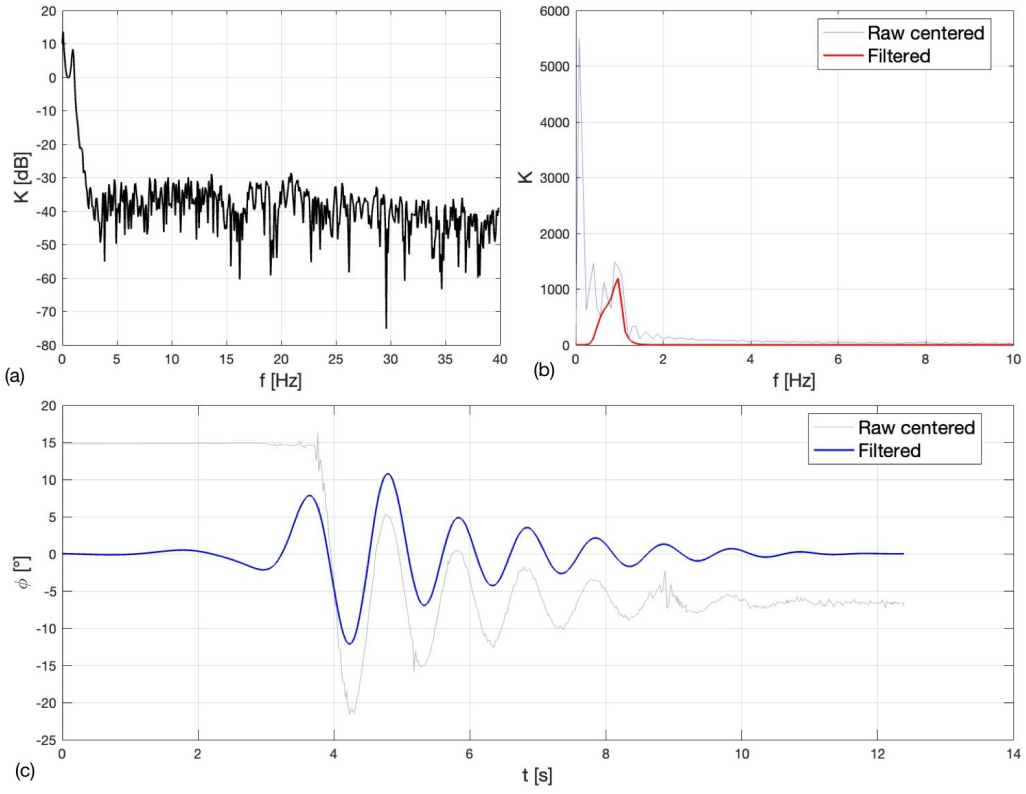

Figure 7. Filtered Angular Signal: Log-Spectrum, Linear Spectrum, and Time-Domain Representations.

7 Conclusion and discussion

The motivation for this experiment was to study the behavior of sailboats. Specifically, the deflection of the mast in steady wind conditions, and the rolling behavior in terms of angle and applied force at the bottom of the mast in the case of a sudden wind lull.
To study those behaviors, we designed a simplified sailboat model made of a mast, hull and keel in order to let it rotate around its bow-stern axis. We added springs to enhance the oscillation and better replicate real world behavior. We placed it in an aquarium filled to the hull with water to simulate the real dynamics of water.

This model allowed us to study the rolling motion by suddenly stopping the wind flow, using an accelerometer and a load cell, on the one hand. On the other hand, it allowed us to study the mast's deflection by blocking the rotation of the boat.

The study of the values obtained proved a sailboat keeps oscillating as an under-damped oscillator for a period of time when the wind suddenly stops. This occurs despite damping by the surrounding water, and proves the necessity of anti-roll devices even in calm conditions. Any future development should take into account the results of experiments similar to this one in counteracting roll.
We also demonstrated that a sailboat's mast can experience deflection akin to a clamped beam subject to point force. This has implications that should be taken into account in the design of masts.

To make further use of our setup, an idea for future improvement would be to test out various sail-mast configurations with various designs and materials and study their behavior. This would help drawing conclusions regarding ideal designs.
Another improvement would be to oscillate the wind force in order to generate dynamical effects on the model. This could prove useful in studying sailboats in extreme conditions, such as storms, where phenomena such as resonance can be observed.
The logical next step towards the goal of this experiment would be the implementation of an active ballast transfer system on a small scale. A setup similar to ours could prove ideal to test the behavior of such a technology at an early stage in its development.

Author contributions

All group members contributed evenly to this project. Imagining the experiment in the earlier phases was a common process. Designing and manufacturing the components was mostly done by Romain, César and Guillaume, while Maxence focused most heavily on the electronics. Understanding and analysing the data was done together, as was the writing of the report. During all phases, we made sure everyone was present to ensure we all fully understood the experiment.

Acknowledgments

We would like to thank the assistants and Dr. Karen Mulleners for the organization of this course and supporting us with precious advice.